JOURNAL OF MATERIALS SCIENCE **34** (1999) 4883–4894

Parameters controlling solidification of molten wax droplets falling on a solid surface

R. BHOLA, S. CHANDRA*
Department of Mechanical & Industrial Engineering, University of Toronto, Toronto, Ontario M5S 3G8, Canada
E-mail: chandra@mie.utoronto.ca

An experimental study was done to identify parameters that determine the shape of splats formed by droplets of paraffin wax impacting and freezing on a polished aluminum surface. Impact velocity was varied from 0.5 to 2.7 m/s and surface temperature from 23 to 73 °C. Droplet impact was photographed, and the splat diameter and liquid-solid contact angle measured from photographs. A simple energy conservation model was used to predict the maximum extent of droplet spread and the rate of droplet solidification. The extent of droplet solidification was found to be too small to affect droplet impact dynamics. Photographs showed liquid recoiling in the droplet center following impact on a cold surface (23 °C); the height of recoil diminished if either substrate temperature or impact velocity was increased. Droplet recoil was attributed to surface tension pulling back the periphery of the splat. Reducing the surface temperature increased surface tension, promoting recoil. At sufficiently large impact velocities droplets fragmented. A model based on the Rayleigh-Taylor instability was used to predict the number of satellite droplets that broke loose after impact.

Nomenclature

a	acceleration of tip of splat
C_d	specific heat of drop
C_s	specific heat of substrate
d_s	diameter of solidified layer
D	splat diameter, measured at the splat-substrate interface
D_0	diameter of spherical droplet
D_{max}	final splat diameter
h	heat transfer coefficient
H	parameter defined in Equation 10
k_d	thermal conductivity of drop
k_s	thermal conductivity of substrate
K	splash parameter ($=We^{0.5}\ Re^{0.25}$)
KE_1	initial kinetic energy
ΔKE	kinetic energy loss due to solidification
L	latent heat of fusion
N	number of satellite droplets formed during droplet break up
s	thickness of solid layer
s^*	dimensionless thickness of solid layer($=s/D_0$)
SE_1	droplet surface energy before impact
SE_2	droplet surface energy after impact
t	time
t^*	dimensionless time ($=V_0t/D_0$)
t_c	droplet deformation time
T_m	droplet melting temperature
T_s	surface temperature
$T_{s,i}$	initial surface temperature
V_0	droplet impact velocity

Greek Symbols

α_d	thermal diffusivity of drop
α_s	thermal diffusivity of substrate
β_d	($=\sqrt{k_d\rho_dC_d}$)
β_s	($=\sqrt{k_s\rho_sC_s}$)
γ	surface tension
λ	wavelength of interfacial waves around the periphery of the droplet
μ	viscosity of drop
ρ_d	density of drop
ρ_s	density of substrate
θ	liquid-solid contact angle
ξ	spread factor ($=D/D_0$)
ξ_{eq}	equilibrium spread factor
ξ_{max}	maximum spread factor
Ψ	normalized residual surface energy ($=SE_2/(KE_1+SE_1)$)

Dimensionless numbers

Bi	Biot number ($=hD_0/k_d$)
Pe	Peclet Number ($=V_0D_0/\alpha_d$)
Pr	Prandtl Number ($=Pe/Re$)
Re	Reynolds Number ($=\rho_dV_0D_0/\mu$)
Ste	Stefan Number ($=C_d(T_m-T_s)/L$)
We	Weber Number ($=\rho_dV_0^2D_0/\gamma$)

* Author to whom all correspondence should be addressed.

1. Introduction

An understanding of the physics controlling impact, spread and solidification of molten droplets on a solid substrate is important in the development of a number of industrial applications. These include spray forming [1], thermal spray coating [2], rapid solidification processing [3], soldering [4] and microfabrication [5, 6]. Control of these processes involves a very large number of parameters (e.g., droplet size, velocity, temperature and degree of solidification; substrate material and temperature) which determine the shape and microstructure of components produced. To date, these variables have been optimized largely on the basis of trial and error from which empirical relationships have been derived. Recent research efforts have been directed at developing computer models capable of predicting the effect of varying process variables on the metallurgical properties of the final product [3, 7]. These models require information on the shapes of individual splats formed by impact and solidification of molten droplets.

Madejski [8] studied the deposition of alumina droplets on a solid surface, and developed a simple analytical model to predict the diameter of a solidified splat. More detailed descriptions of droplet impact dynamics are available from numerical models based on a solution of the Navier-Stokes equations [4, 9–12]. A few experimental studies have been done to directly observe droplet impact and solidification. Inada [13] measured surface temperature variation under a molten lead droplet falling on a cold plate, and determined that the droplet cooling rate was a function of impact velocity. Watanabe *et al*. [14] observed the impact of *n*-cetane and *n*-eicosane (hydrocarbons with melting points of 17 and 36 °C respectively) on a cold surface and concluded that solidification had little influence on droplet deformation in their experiments. Inada and Yang [15] used holographic interferometry to observe droplet-substrate contact during impact of lead droplets on a quartz plate. Fukanuma and Ohmori [16] photographed the impact of 2–4 mm diameter tin and zinc droplets on a stainless steel surface, and also found that droplet spreading preceded freezing. Kang *et al*. [17] studied, using both experiments and numerical models, the solidification of two molten lead droplets impacting sequentially one on top of the other. They demonstrated that thermal contact resistance at the splat-substrate interface, and between the two splats, influences droplet cooling rate and grain structure. Theoretical and experimental studies done by Bennett and Poulikakos [18] on the impact and solidification of liquid metal droplets on a cold surface showed that the thermal conductivity of the substrate significantly affect the cooling of the splat.

Most laboratory studies of droplet impact have been done using metal or hydrocarbon droplets 2–4 mm in diameter, impacting at velocities of 1–3 m/s, which are easy to generate and observe. However practical applications encompass a very large range of droplet sizes (from ∼10 μm to ∼1 mm), materials (waxes, polymers, metals, ceramics), and impact velocities (∼1–1000 m/s). We therefore need to be able to scale information obtained from controlled laboratory investigations; this may be done if experimental results are expressed in terms of dimensionless parameters that control droplet impact and solidification. We undertook this study to investigate the relative importance of the many different parameters that may be relevant.

Experiments were done using paraffin wax droplets dropped onto an aluminum surface. Paraffin wax was selected for two reasons. Firstly, solidification of wax droplets is of practical interest; inkjet printers modified to generate wax droplets have been used for fabrication of small structures [5]. Secondly, wax proved to be an ideal subject for laboratory experiments; it is easy to melt and form into uniform sized droplets, yet has a high enough melting point (∼70 °C), that freezing is rapid during impact on a surface at room temperature. Paraffin wax is opaque when solid but becomes a transparent liquid on melting, allowing solidification to be observed directly. It has a low thermal conductivity so that—as will be demonstrated—the effect of thermal contact resistance between the drop and the substrate is negligible, greatly simplifying the analysis of droplet solidification. An aluminum surface was used since it has high thermal conductivity, and may be reasonably assumed isothermal during droplet impact. We varied droplet impact velocity (0.5–2.7 m/s) and surface temperature (23–73 °C). Initial droplet diameter (3.0 mm), droplet temperature (73 °C), and ambient air temperature (∼23 °C) were held constant. We photographed impacting droplets, and measured droplet spread diameters and liquid-solid contact angle from these photographs. We also measured surface temperature variation under an impacting drop, and estimated the thermal contact resistance from these measurements. Our objective was to develop simple models to predict the extent of droplet spread, the effect of substrate temperature on droplet impact dynamics, and conditions leading to droplet break up.

2. Experimental apparatus

Experiments were done using droplets of paraffin wax (product code 1260, IGI International Waxes Ltd.). Temperature measurements during phase change showed a melting point of 70 ± 1 °C. We formed droplets of molten wax by letting them detach from the tip of a stainless steel needle. The surface tension of wax at room temperature (approximately 23 °C) was measured by equating the measured weight of droplets to the force attaching them to the needle tip, whose diameter was known; the calculated value of surface tension is listed in Table I. Other properties were obtained from the manufacturer and are also listed in Table I.

TABLE I Properties of paraffin wax

T_m (°C)	γ (N/m)	ρ (kg/m^3)	L (J/kg)	C (J/kg K)	α (m^2/s)	μ (Ns/m^2)
70	22.4×10^{-3}	771	226×10^3	2.56×10^3	1.2×10^{-7}	5.4×10^{-3}

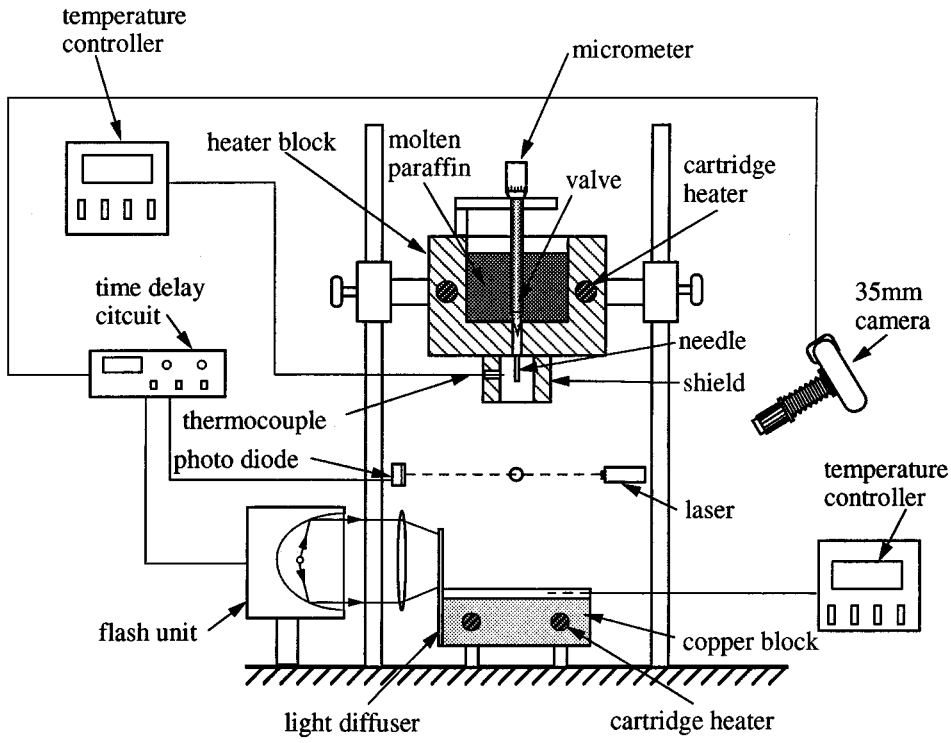

Figure 1 Schematic diagram of the experimental apparatus.

Physical properties were assumed constant and the tabulated values used in all subsequent calculations.

Fig. 1 shows the apparatus used to form wax droplets and photograph their impact on a solid surface. Paraffin wax was melted in a 50.8 mm diameter and 38.1 mm deep cavity machined in an aluminum block, in which were inserted two 60 W cartridge heaters regulated by an electronic temperature controller. The temperature of the block was held at 73 °C (2° above the maximum melting point of the wax). We estimated, based on heat transfer calculations, that the droplet would cool by approximately 1 °C during its flight; it was therefore still liquid, at its melting point, prior to impact. A 1.6 mm outside diameter stainless steel needle was press fitted into a hole drilled in the bottom of the cavity, through which molten wax was forced by gravity. The flow rate was regulated by a valve mounted on a micrometer stage, that partially blocked the entrance to the needle. Liquid accumulated at the tip of the needle until its weight exceeded the surface tension force supporting it, at which time it detached and fell onto the test surface. The needle was shielded from the surrounding colder air to prevent cooling of the droplet before detaching. Wax droplets 3.0 ± 0.01 mm in diameter formed and detached at a rate of approximately one per minute.

The aluminum block was mounted on a frame so that it could be raised to a height of up to 360 mm above the test surface, corresponding to a droplet impact velocity of 2.7 m/s. The test surface used was a 50.8 mm square by 6.35 thick aluminum plate polished with 600 grit emery cloth and metal polish. This surface was mounted on a copper block heated by two cartridge heaters, whose temperature was controlled by a second temperature controller. Surface temperature was measured by a chromel-alumel thermocouple inserted in a hole in the test surface.

Wax droplets falling on a clean aluminum surface froze and adhered to the surface, and could be removed only by being scraped off, which damaged the surface. We prevented adhesion by wiping the surface prior to depositing a drop with a cotton cloth that had been lightly dampened with a trace of SAE 20 lubricating oil. The oil layer left behind on the surface was so thin as not to be visible, and did not alter the thermal properties of the test surface. Measurements of the surface temperature variation under an impacting drop showed no change when the oil was applied.

Photographs of droplet impact were taken using a single shot flash photographic method, in which an electronic flash unit was used to take a single 35 mm photograph of a droplet at one instant after impact. By advancing the time at which the drop was photographed in small increments (0.1 ms), the entire impact process could be recreated from images of droplets at different stages of impact. Droplets falling towards the surface passed through the beam of a 0.5 MW He-Ne laser placed above the test surface. Interruption of the laser beam was detected by a photo diode, sending a signal to the time delay circuit. This circuit opened the shutter of a Nikon F-3 camera, and after a preset time delay triggered a flash unit which provided diffused backlighting to photograph the droplet. The flash had a maximum duration of 8 μs, short enough to effectively freeze droplet motion at any stage of impact. A detailed description of the photographic method has been given by Chandra and Avedisian [19].

Measurements of droplet dimensions were made from photographs, using a photograph of a 6.35 mm steel ball bearing as a calibration scale. A photographic enlarger was used to project images of droplets on a white surface, from which measurements of droplet diameter were made with a resolution of ±0.01 mm.

To confirm that the thermal contact resistance between wax droplets and the substrate was negligible, we measured surface temperature variation during droplet impact using a commercially available chromel-alumel thermocouple (E-12-3-K, Nanmac Inc., Framingham, MA) placed at the point of impact. The response time of the thermocouple, specified by the manufacturer, was 10 μs. The thermocouple was inserted vertically through the test surface and the junction ground flush with the surface. The thermocouple output was amplified and recorded during droplet impact using a data acquisition system.

3. Results and discussion

Fig. 2 shows photographs of successive stages of impact of wax droplets with an initial velocity of 1 m/s and temperature of 73 °C, on an aluminum surface at 23 °C. The time of each photograph, measured from the instant of impact ($t = 0$) is indicated. The upper half of the droplets appears darker than the lower half because the test surface was reflected in the droplet. A small satellite drop can also be seen in some frames, which formed during droplet detachment from the needle tip. Immediately after the droplet touched the surface liquid jetted away from the point of impact. The droplet spread on the surface, reaching its maximum extension at $t \approx 3.0$ ms. Surface tension forces pulled the liquid back, reducing the splat diameter. The wax was transparent when liquid, and turned opaque as it solidified; solidified portions of droplets therefore appear darker in the photographs. There is evidence of droplet solidification as early as $t = 7.5$ ms. The periphery of the droplet appear to have frozen by $t = 9.5$ ms, as indicated by its irregular shape; surface tension forces would have smoothed out the irregularities if the edge was still fluid. However, surface tension continued to act on the center portion of the droplet which was still liquid, pulling it back so that it eventually recoiled off the surface ($t = 14.5$ ms). The droplet then subsided under its own weight, eventually reaching its equilibrium shape by approximately $t = 20$ ms.

The effect of changing substrate temperature on droplet impact dynamics is illustrated in Fig. 3, which shows droplets impacting with a velocity of 0.8 m/s on surfaces maintained at three different temperatures (T_s): 23, 40 and 73 °C. Each column of photographs shows successive stages of droplet deformation on a surface at a given temperature. Measurements of the evolution of splat diameter (D), made from these photographs, are shown in Fig. 4. For $T_s = 73$ °C the droplet and surface were at the same temperature, and there was no solidification; impact was isothermal and the droplet remained liquid during the entire spreading process. Photographs of impact at lower surface temperatures (see Fig. 3, $T_s = 40$ and 23 °C) show the effect that cooling the liquid had on droplet spreading. Lowering surface temperatures can be seen to reduce the rate of splat spreading (see Fig. 3, $t = 1.5$ ms). The diameter of a drop impacting on a surface at 23 °C reached a maximum (D_{max}) at $t = 5.7$ ms, after which surface tension forces drew the edges back in, making the drop recoil ($t = 18.2$ ms). The height of droplet recoil was larger in these photographs than in Fig. 2, where the impact velocity was greater (1 m/s); the recoil diminished as surface temperature was increased. The recoil of the droplet produced oscillations in the measured value of D, visible in Fig. 4. On a surface at 23 °C the equilibrium splat diameter (D_{eq}, measured at $t > 100$ ms) was significantly smaller than D_{max}. At higher surface temperatures, when droplet recoil was restricted, the difference between D_{max} and D_{eq} decreased; only a very small recoil can be detected for $T_s = 73$ °C (see Fig. 4).

The final splat shape was characterized by measuring the equilibrium splat diameter (D_{eq}) and nondimensionalizing it by the initial droplet diameter (D_0) to obtain the "equilibrium spread factor" ($\xi_{eq} = D_{eq}/D_0$). Fig. 5 shows the variation of ξ_{eq} with impact velocity (V_0), for impact on both a cold surface ($T_s = 23$ °C) and a hot surface ($T_s = 73$ °C). The effect of surface temperature on equilibrium splat shape was evident for $V_0 < 1.8$ m/s; at higher velocities ξ_{eq} was independent of T_s. Data for ξ_{eq} show increased scatter as V_0 became larger, because splat edges began to fragment, making repeatable measurements more difficult.

We can predict the equilibrium splat diameter (D_{eq}) for the case of isothermal droplet impact using a simple energy conservation model developed by Pasandideh-Fard *et al.* [20]. The model predicts D_{max} rather than D_{eq} for a liquid droplet impacting on a solid substrate. However, for $T_s = 73$ °C we observed that $D_{max} \approx D_{eq}$ (see Fig. 4) so that the analysis is valid for estimating D_{eq}. D, normalized by D_{max}, varied with dimensionless time ($t^* = tV_0/D_0$) as:

$$\frac{D}{D_{max}} = \sqrt{\frac{3}{8}t^*} \tag{1}$$

From Equation 1, the dimensionless time required for the droplet to reach its maximum spread ($D = D_{max}$) is $t^* = 8/3$, and is independent of impact velocity. Fig. 6 shows the measured variation of D/D_{max} during spreading of droplets with three different impact velocities on a surface at 73 °C (so that impact was isothermal). Our observations confirmed that in the range of velocities used in our experiments the time for a liquid drop to reach equilibrium was reasonably predicted by $t^* = 8/3$. Droplet recoil was negligible; therefore, irrespective of impact velocity, $\xi_{eq} \approx \xi_{max}$.

The maximum spread diameter of a droplet was predicted by Pasandideh-Fard *et al.* [20] by calculating the droplet energy before and after impact. The initial kinetic energy (KE_1) and surface energy (SE_1) of a liquid droplet before impact are:

$$KE_1 = \left(\frac{1}{2}\rho V_0^2\right)\left(\frac{\pi}{6}D_0^3\right) \tag{2}$$

$$SE_1 = \pi D_0^2 \gamma \tag{3}$$

After impact, when the droplet is at its maximum extension, the kinetic energy is zero and the surface energy is:

$$SE_2 = \frac{\pi}{4}D_{max}^2\gamma(1 - \cos\theta) \tag{4}$$

The work done in deforming the droplet against viscosity is [20]:

$$W = \frac{\pi}{3}\rho V_0^2 D_0 D_{max}^2 \frac{1}{\sqrt{Re}} \tag{5}$$

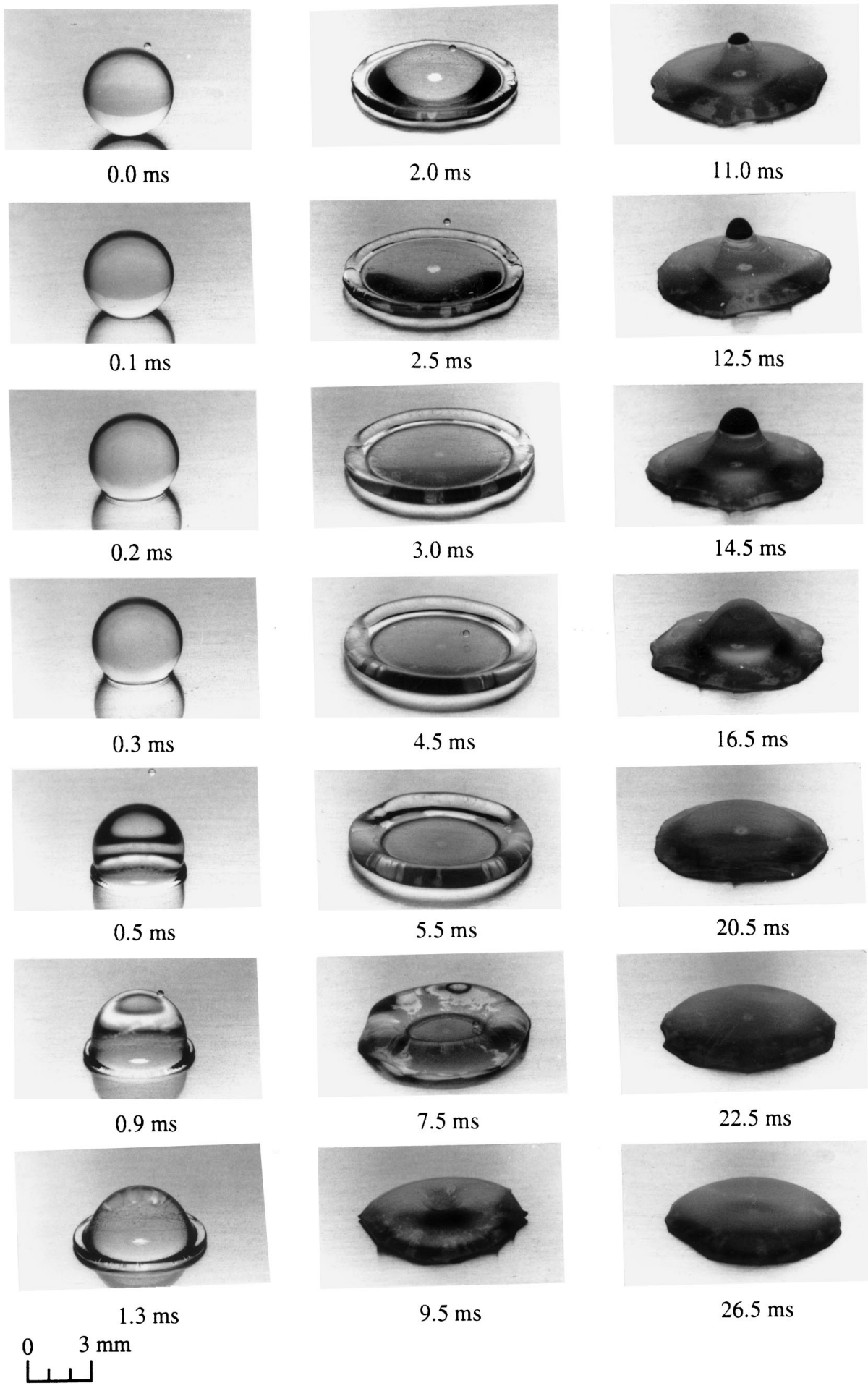

Figure 2 Impact of a molten wax droplet with velocity 1.0 m/s on an aluminum surface at 23 °C.

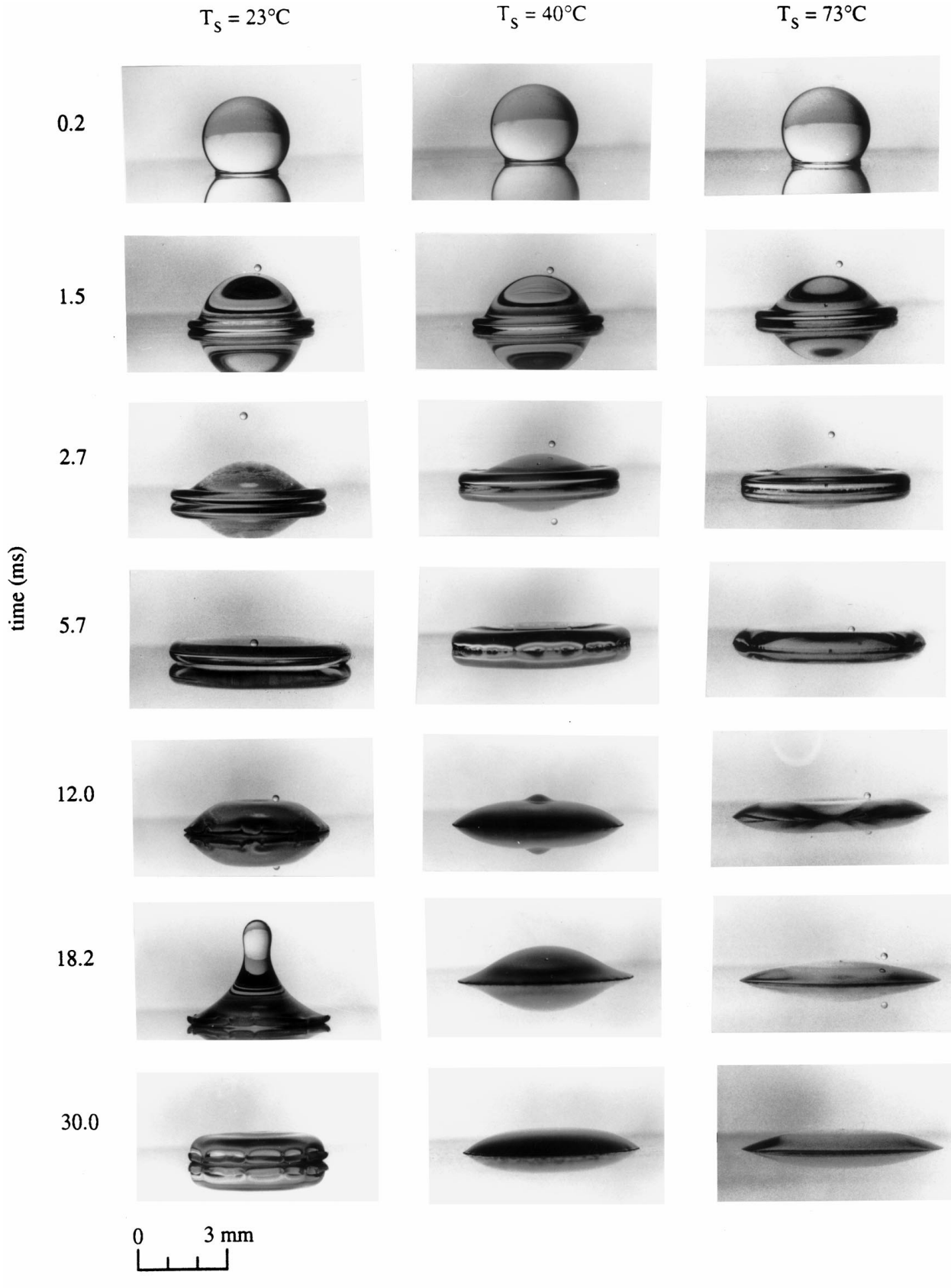

Figure 3 Impact of a molten wax droplet with velocity 0.8 m/s on an aluminum surface at temperature T_s.

Substituting Equations 2–5 in the energy balance equation $KE_1+SE_1 = SE_2+W$ yields an explicit expression for the maximum spread factor [20]:

$$\xi_{\max} = \frac{D_{\max}}{D} = \sqrt{\frac{We + 12}{3(1-\cos\theta) + 4(We/\sqrt{Re})}} \quad (6)$$

For the case that $We \gg \sqrt{Re}$, and also $We \gg 12$, Equation 6 can be further simplified to:

$$\xi_{\max} = 0.5Re^{0.25} \quad (7)$$

For the range of impact velocities in our experiments (0.5 m/s $< V_0 <$ 2.7 m/s), we calculated that

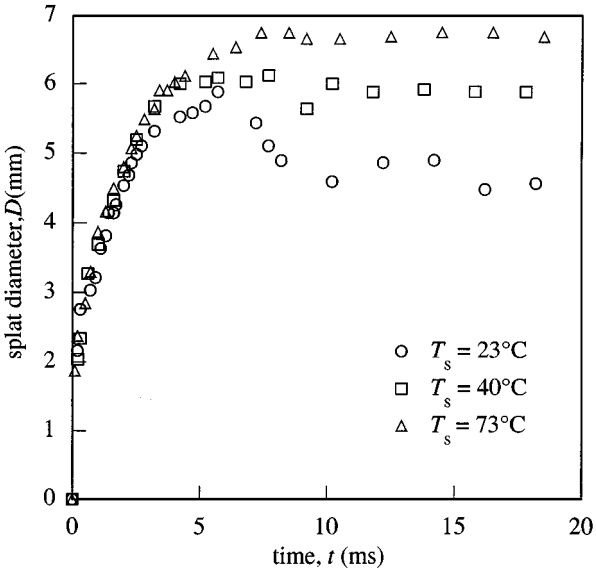

Figure 4 Splat diameter evolution for wax droplets impacting with a velocity of 0.8 m/s on an aluminum surface at temperature T_s.

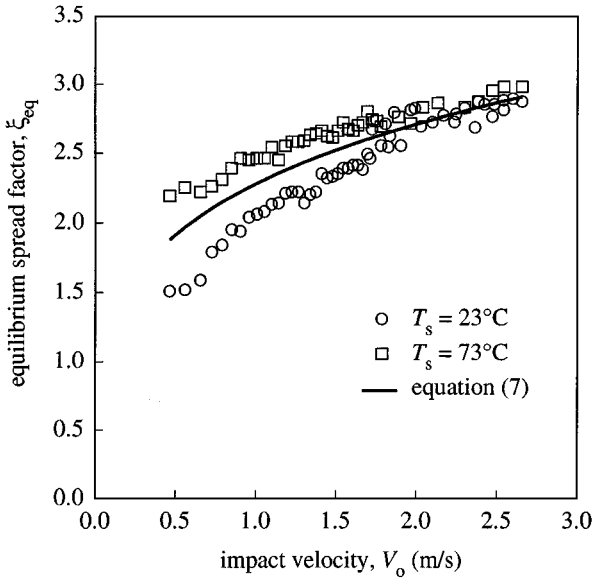

Figure 5 Variation of equilibrium spread factor with impact velocity, for impact of wax droplets on an aluminum surface at temperature T_s.

$26 < We < 698$ and $214 < Re < 1114$. We found predictions from Equations 6 and 7 to be always very close to each other irrespective of the value of θ. Therefore, only Equation 7 was used to calculate values of ξ_{max} that are plotted in Fig. 5. For droplets impacting on a surface at 73 °C, there was no recoil of the splat (see Fig. 6), and $\xi_{eq} \approx \xi_{max}$; reasonable agreement is seen between Equation 7 and measurements of ξ_{eq} for $T_s = 73$ °C. Predictions were less accurate at low velocities where the assumption of boundary layer flow made in deriving Equation 5 was not satisfied; reasons for the error have been discussed by Pasandideh-Fard *et al.* [20]. Calculations of ξ_{max} from the expression proposed by Madejski [8] gave values approximately twice those obtained from Equation 7.

At low impact velocities ($V_0 < 1.8$ m/s), cooling the substrate to 23 °C reduced the value of ξ_{eq}, making it less than it was for a droplet impacting on a surface at

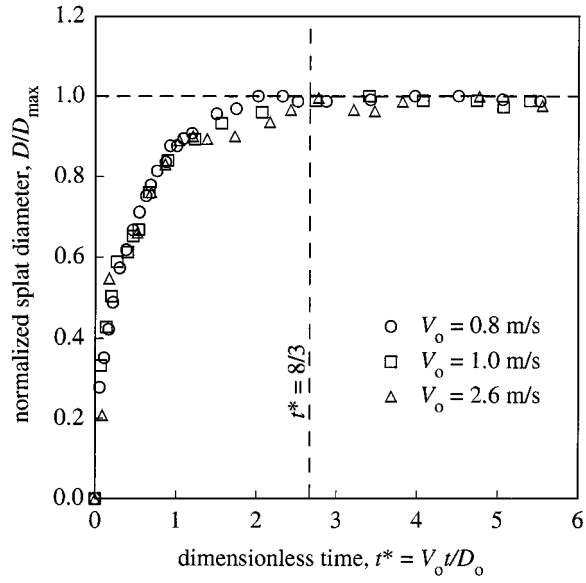

Figure 6 Normalized splat diameter evolution for wax droplets impacting on a hot aluminum surface ($T_s = 73$ °C) with velocity V_0.

73 °C (see Fig. 5). Lowering substrate temperature can influence droplet impact dynamics through two mechanisms: firstly, solidification of the liquid adjacent to the substrate can restrict spreading; secondly, even if the liquid does not completely solidify, cooling it to near the freezing temperature can greatly increase its surface tension and viscosity. We will use simple models of droplet impact and solidification to compare the relative importance of these two effects.

The effect of droplet solidification on the maximum spread diameter can be determined by modifying the energy balance model discussed above, assuming that all the kinetic energy stored in the solidified layer is lost. If the solidified layer has thickness s and diameter d_s when the splat is at its maximum extension, then the loss of kinetic energy is approximated by:

$$\Delta KE = \left(\frac{\pi}{4} d_s^2 s\right)\left(\frac{1}{2}\rho V_0^2\right) \qquad (8)$$

d_s varies between 0 and D_{max}; a reasonable estimate is $d_s \sim D_{max}/2$. We can estimate the thickness of the solidified layer (s) by making the following assumptions: the droplet is at its melting point (T_m); heat transfer to the droplet is by one-dimensional heat conduction into a semi-infinite body; the test surface is isothermal; and that the thermal resistance at the splat-substrate interface is negligible. The first three assumptions are manifestly plausible. Droplets were maintained at their melting point in our experiments. The thermal penetration depth during droplet impact equals, to within an order of magnitude, $\sqrt{\alpha_d t}$; for $t = 10$ ms, this equals 35 μm, which is much less than the droplet diameter. The droplet can therefore be assumed to be semi-infinite in extent, and heat transfer to be one-dimensional. Finally the aluminum test surface can be assumed to be isothermal because T_s was estimated to change only by about 1 °C during droplet impact, assuming the drop and surface to be semi-infinite bodies suddenly brought in contact [21].

The fourth assumption, that contact resistance at the interface is negligible, is valid if the Biot number ($Bi = hD_0/k_d$) is large. We estimated the magnitude of the heat transfer coefficient (h) at the liquid-solid interface by measuring substrate temperature fluctuation during droplet impact. Since the temperature change of an aluminum surface was too small (<1 °C) to measure accurately, we used a stainless steel surface, identical in size and surface finish to the aluminum surface, to conduct our temperature measurements. We assumed that the thermal contact resistance between the two surfaces and impacting wax droplets would of the same order of magnitude. Fig. 7 shows the surface temperature variation during the impact of a droplet on a surface initially at 24 °C; the temperature increased by approximately 6 °C in the 0.25 ms following impact. To calculate the coefficient of heat transfer between the droplet and substrate, we used an analytical model of heat transfer between two semi-infinite bodies brought instantaneously in contact, with a thermal resistance at the interface. If heat transfer is by one-dimensional heat conduction, the surface temperature variation is given by [22]:

$$T_s = T_{s,i} + \frac{\beta_d}{\beta_d + \beta_s}(T_m - T_{s,i}) \times \left\{1 - \exp\left(H^2\alpha_s t\right)\mathrm{erfc}(H\sqrt{\alpha_s t})\right\} \quad (9)$$

where

$$\beta_d = \sqrt{k_d\rho_d C_d}, \qquad \beta_s = \sqrt{k_s\rho_s C_s}$$

and

$$H = \frac{\beta_d + \beta_s}{k_s\beta_d}h \quad (10)$$

The curve represented by Equation 9 was fitted to our experimental data, using a least squares fit, to determine the value of h that gave the best match. Fig. 7 shows the closest fit, obtained using a value of $h = 6 \times 10^4$ W/m^2 K. The corresponding value of $Bi = 760$, which is much greater than unity. It is therefore reasonable to assume perfect contact at the droplet-substrate interface.

If heat transfer is by one-dimensional heat conduction, the solid layer thickness (s) increases with time as [21]:

$$s = \sqrt{2\alpha_d t\, Ste} \quad (11)$$

where the Stefan number (Ste) is defined as $Ste = C_d(T_m - T_s)/L$. Substituting $t = (8/3)(D_0/V_0)$ in Equation 11 gives an estimate of the thickness of the solid layer formed in the time the droplet takes to reach its maximum spread:

$$\frac{s}{D_0} = \sqrt{\frac{16}{3}\frac{Ste}{Pe}} \quad (12)$$

where Pe is the Peclet number ($Pe = V_0D_0/\alpha_d$). The energy balance equation, modified to account for the loss of kinetic energy due to solidification, is: $KE_1 + SE_1 = SE_2 + W + \Delta KE$. Substituting in this Equations 2–5, 8, and 12, and assuming $d_s \sim D_{max}/2$, gives an expression for the maximum spread factor for a droplet that is solidifying during impact:

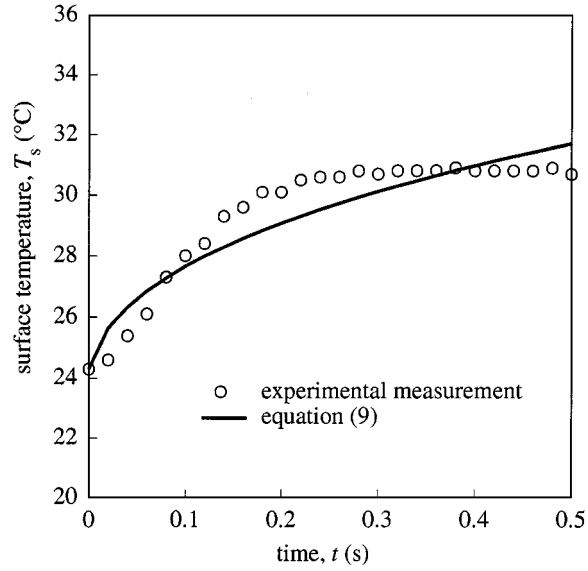

Figure 7 Surface temperature variation during the impact of a wax droplet with a velocity of 1 m/s on a stainless steel surface.

$$\xi_{max} = \sqrt{\frac{We + 12}{3(1 - \cos\theta) + 4(We/\sqrt{Re}) + We\sqrt{(3Ste)/(4Pe)}}} \quad (13)$$

For $We \gg \sqrt{Re}$ and $We \gg 12$, which was the case in our experiments, we may simplify this equation to give:

$$\xi_{max} = \sqrt{\frac{\sqrt{Re}}{4 + \sqrt{(3Ste)/(4Pr)}}} \quad (14)$$

in which the Prandtl number, $Pr = Pe/Re$. If $Ste/Pr \ll 1$, values of ξ_{max} predicted by Equation 14 approach those obtained from Equation 7, i.e., the extent of solidification is too small to have a significant effect on droplet spread. This was indeed found to be the case in our experiments, where $Ste = 0.6$, $Pr = 58$, and $Ste/Pr = 0.01$. Therefore, in the time taken for the droplet to spread, the thickness of the solidified layer was not sufficient to significantly impede motion of the liquid. Inspection of Fig. 2 confirms that there was no solidification in the time that the droplet was spreading ($t < 3$ ms). The first evidence of solidification is visible in a later frame, when $t \approx 7.5$ ms. Note that Equation 11 neglects any effects of undercooling and thermal contact resistance; it therefore gives an upper bound to the thickness of the solidified layer. In reality undercooling of the molten liquid below its freezing point may further reduce the value of s.

Since solidification was insufficient to restrict droplet spreading, changes in physical properties appear to be the main reason that substrate temperature affects

equilibrium splat diameter: in particular, viscosity and surface tension increase when the liquid temperature is lowered [23]. Greater liquid viscosity would increase the energy dissipated during droplet deformation and recoil, and we would therefore expect the height of recoil to be less on a cold surface than on a hot surface. We observed the reverse effect in our experiments (see Fig. 3), leading us to conclude that an increase in surface tension was the main result of cooling the droplet. We had no method of directly measuring surface tension, which could vary both with time and location in the droplet. However, we could estimate the residual surface energy (SE_2) after the droplet has finished spreading using Equation 4 and experimental measurements of the liquid-solid contact angle (θ). Close inspection of the photographs in Fig. 3 shows that θ increases as surface temperature is reduced (e.g., see Fig. 3, t = 5.7 ms). SE_2 was therefore greater on a cold surface, increasing the height of recoil as surface tension forces pulled back the drop. Experiments on impact of water droplets on a solid surface [20] have shown that reducing the contact angle by addition of a surfactant to water can reduce droplet recoil after impact.

The variation in liquid-solid contact angle was measured from enlargements of the photographs in Fig. 3; results are shown in Fig. 8. At the instant of contact $\theta \approx 130^\circ$, irrespective of surface temperature. However, on a surface with $T_s = 23\,^\circ$C θ progressively increased as the liquid cooled. Eventually the periphery froze and the contact angle remained fixed at approximately 155 °C. Conversely, on a surface with $T_s = 73\,^\circ$C, θ decreased as the droplet spread, eventually reaching its equilibrium value of 25°. At the moment of maximum droplet spread ($t \approx 6$ ms) there was a large difference in contact angle at the three surface temperatures ($\theta = 155^\circ$ for $T_s = 23^\circ$C; $\theta = 90^\circ$ for $T_s = 40\,^\circ$C; $\theta = 80^\circ$ for $T_s = 73\,^\circ$C). Measured contact angles did not vary significantly with impact velocity over the range of our measurements.

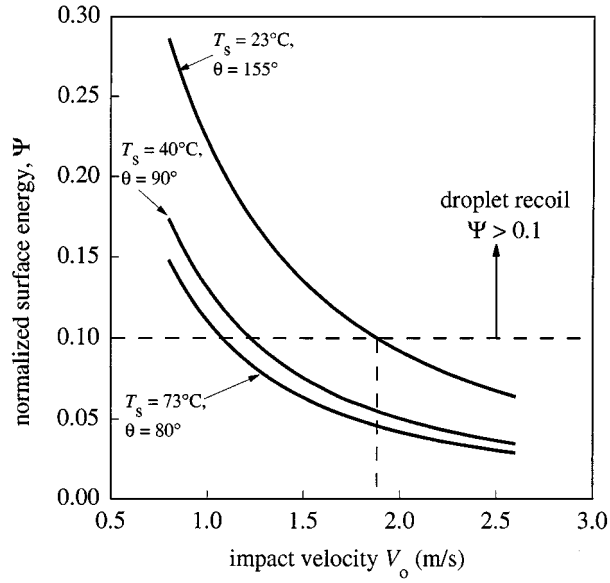

Figure 9 Normalized residual surface energy variation with impact velocity for droplet impact on a surface at temperature T_s.

Dividing the surface energy at the end of impact (SE_2) by the total initial energy of the droplet ($KE_1 + SE_1$), we can define the normalized residual surface energy:

$$\Psi = \frac{SE_2}{KE_1 + SE_1} = \left(1 + \frac{4}{3}\frac{We}{(1-\cos\theta)\sqrt{Re}}\right)^{-1} \tag{15}$$

Values of Ψ calculated from Equation 15 are shown in Fig. 9 as a function of impact velocity for three different values of θ (155°, 90° and 80°), corresponding to the three surface temperatures at which contact angle measurements were made (T_s = 23, 40 and 73 °C). Impact velocity was found to reduce the equilibrium spread factor of droplets impacting on a surface at 23 °C for $V_0 > 1.8$ m/s (see Fig. 5). This velocity corresponds

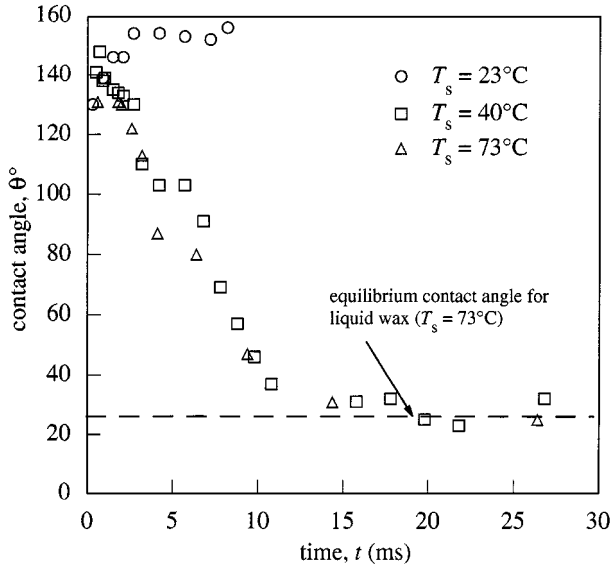

Figure 8 Contact angle variation during spreading of wax droplets impacting with a velocity of 0.8 m/s on an aluminum surface at temperature T_s.

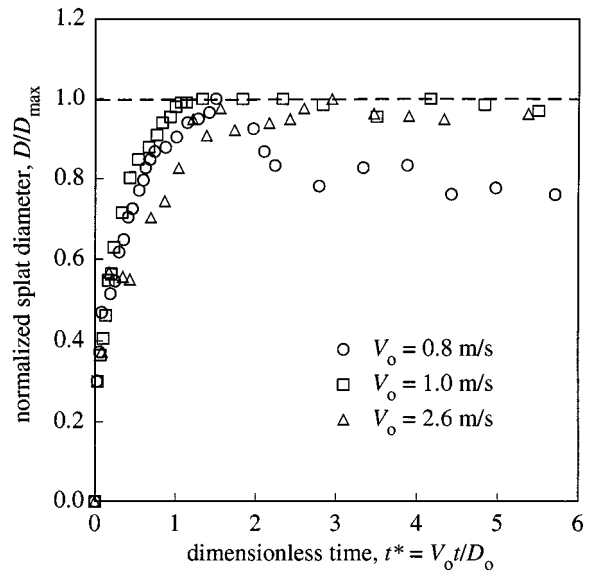

Figure 10 Normalized splat diameter evolution for wax droplets impacting on a cold aluminum surface ($T_s = 23\,^\circ$C) with velocity V_0.

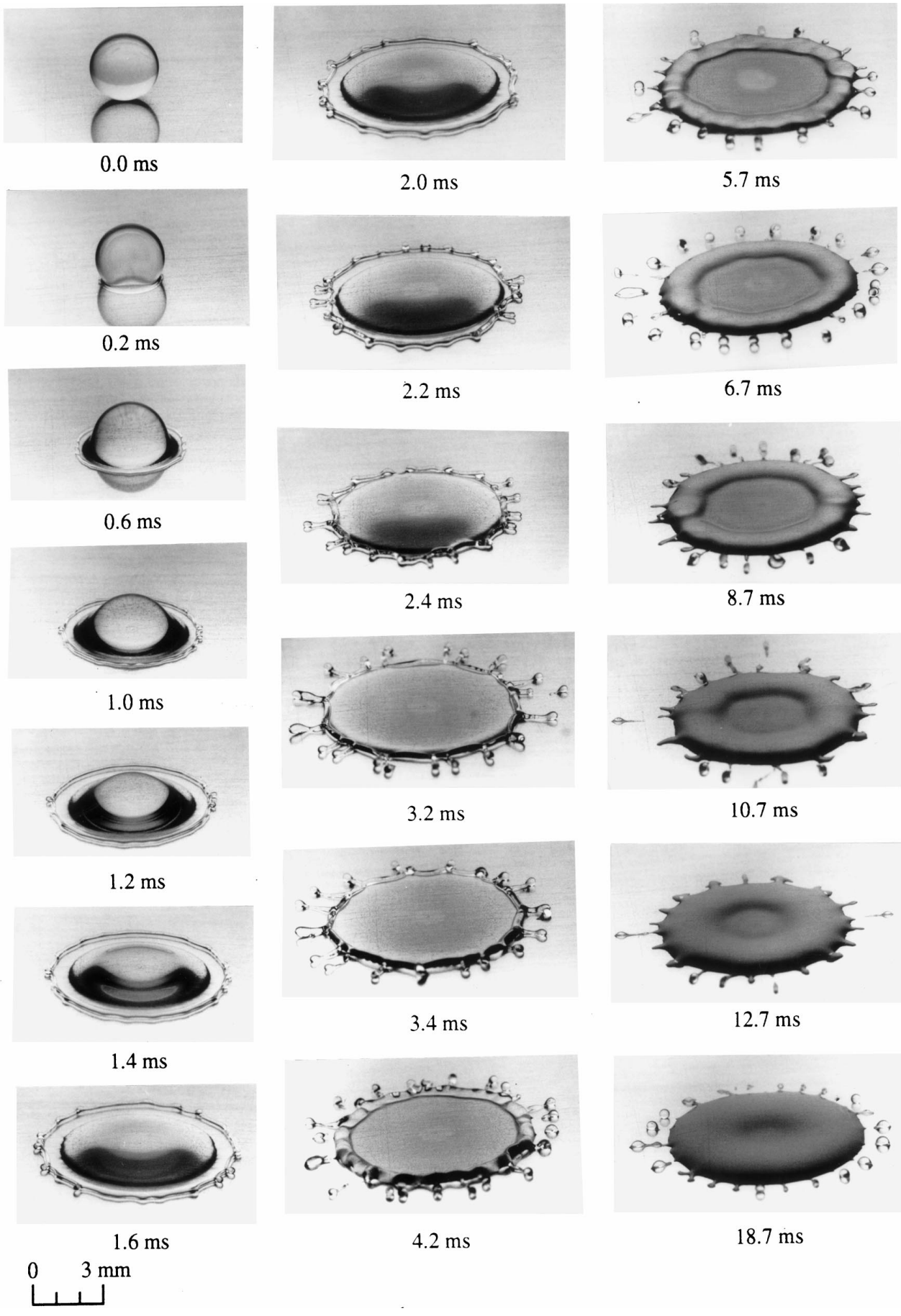

Figure 11 Breakup of a molten wax droplet following impact with a velocity of 2.2 m/s on an aluminum surface at 23 °C.

to $\Psi = 0.1$ for $T_s = 23\,^{\circ}$C (see Fig. 9): i.e., retaining 10% of the initial energy is sufficient to cause a droplet to recoil after impact. Measurements of splat diameter evolution for droplets landing on a surface at 23 °C show a large recoil at $V_0 = 0.8$ m/s (Fig. 10) so that the equilibrium spread factor $\xi_{eq} < \xi_{max}$. However, as impact velocity increased most of the initial energy of the droplet was dissipated by viscous forces, leaving less stored as surface energy: no recoil can be seen for $V_0 = 2.6$ m/s in Fig. 10 so that $\xi_{eq} \approx \xi_{max}$. Ψ decreased as surface temperature was raised and the contact angle θ became smaller. At $T_s = 73\,^{\circ}$C, the condition $\Psi < 0.1$ corresponds to $V_0 > 1.1$ m/s. We would therefore expect to see no recoil at higher impact velocities. Fig. 6 confirms that very little recoil was seen for droplets impacting on a surface at 73 °C, even at very low impact velocities.

Increasing impact velocity eventually caused the droplet to fragment. Fig. 11 shows photographs of a droplet impacting with a velocity of 2.2 m/s on a surface at 23 °C. An instability can be seen developing around the periphery of the drop soon after impact (see $t = 0.6$ ms) in the form of small waves. These waves grew larger, with their tips eventually detaching in the form of small droplets. The number of droplets varied from 18–22, spaced evenly around the perimeter of the drop.

Mundo *et al.* [24] and Stow and Hadfield [25] studied the splashing of liquid drops. They both observed that splashing occurred when the splash parameter $K = \sqrt{We\sqrt{Re}}$ exceeded a critical limit, whose value depended on the solid surface roughness. For water and ethanol drops impacting on a smooth surface they found experimentally [24] that $K = 57.7$. In our experiments we found that the impact velocity required to produce splashing was higher on a hot surface than on a cold surface: for $T_s = 23\,^{\circ}$C, $K = 102$ and for $T_s = 73\,^{\circ}$C, $K = 137$. Savic and Boult [26] had previously observed in their experiments on the impact of wax droplets on a cold surface that raising the droplet temperature delayed the onset of droplet break up. They concluded that solidification of the splat assists droplet disintegration. Solidification of the splat near its center, which contacts the substrate first, retards its spread and makes it easier for the droplets to break free from the periphery.

Allen [27] suggested that droplet splashing is an example of Rayleigh-Taylor instability, caused by a denser fluid being accelerated into a lighter one. If the magnitude of acceleration is a, the wavelength of the interfacial waves is [27]:

$$\lambda = 2\pi\sqrt{\frac{3\gamma}{a\rho}} \tag{16}$$

The number of waves (N) around the perimeter of the drop then equals:

$$N = \frac{\pi D_{max}}{\lambda} = D_{max}\sqrt{\frac{a\rho}{12\gamma}} \tag{17}$$

A simple estimate of the acceleration of the tip of the spreading liquid jet is $a \sim V_0^2/D_0$. Substituting in Equation 17, and using Equation 7 to calculate D_{max} gives:

$$N = \sqrt{\frac{We\sqrt{Re}}{48}} = \frac{K}{4\sqrt{3}} \tag{18}$$

For the conditions of Fig. 11 ($We = 500$, $Re = 942$) Equation 18 predicts $N = 18$, which agrees closely with the 19 droplets observed breaking loose from the splat when it was at its maximum extension (see Fig. 11, $t =$ 3.2 and 3.4 ms).

4. Conclusions

The impact and solidification of molten wax droplets on an aluminum surface was studied experimentally. We photographed impacting droplets, and measured splat diameters and liquid-solid contact angles during spreading. The principal parameters varied were impact velocity (0.5–2.7 m/s) and surface temperature (23–73 °C).

Measurements of surface temperature variation under an impacting drop showed that the thermal contact resistance was negligible. A simple model based on energy conservation was used to predict the maximum extent of liquid droplet spread. Predictions from the model were found to agree well with experimental measurements of droplet impact on a surface at 73 °C, for which impact was isothermal. On a surface at 23 °C, the equilibrium splat diameter was smaller than it was on a hot surface. The extent of droplet solidification was found to be too small to affect droplet impact dynamics. However it was shown that if more that 10% of the initial droplet energy remained as surface energy after impact, the droplet recoiled and the equilibrium splat diameter was reduced. Increasing impact velocity led to droplet break up; reducing substrate temperature was found to promote break up. A model based on the Rayleigh-Taylor instability was used to predict the number of satellite droplets that broke loose after impact.

References

1. R. E. LEWIS and A. LAWLEY, "P/M in Aerospace and Defense Technologies" (Metal Powders Industries Federation, Princeton, 1991) pp. 173–184.
2. M. VARADELLE, A. VARADELLE, A. C. LEGER, P. FAUCHAIS and D. GOBIN, *Journal of Thermal Spraying Technology* **4**(1) (1994) 50–58.
3. E. GUTIERREZ-MIRAVETE, "Rapid Solidification Technology" (Technomic Publishing Co., Lancaster PA, 1993) pp. 3–70.
4. J. M. WALDVOGEL and D. POULIKAKOS, *International Journal of Heat and Mass Transfer* **40** (1997) 295–309.
5. F. GAO and A. A. SONIN, *Proceedings of the Royal Society A* **444** (1994) 533–554.
6. C.-A. CHEN, J.-H. SAHU, J.-H. CHUN and T. ANDO, in "Science and Technology of Rapid Solidification and Processing," edited by M. A. Otooni (Kluwer Academic Publishers, Netherlands, 1995) pp. 123–134.
7. P. MATHUR and D. APELIAN, "Powder Metallurgy: An Overview" (Institute of Metals, London, 1991) pp. 22–44.
8. J. MADEJSKI, *International Journal of Heat and Mass Transfer* **19** (1976) 1009–1013.

9. G. TRAPAGA, E. F. MATTHYS, J. J. VALENCIA and J. SZEKELY, *Met. Trans. B* **23B** (1992) 701–918.
10. H. LIU, E. J. LAVERNIA and R. RANGEL, "Deformation and Interaction Behavior of Molten Droplets Impinging on a Flat Substrate in Plasma Spray Process," Proceedings of the 6th National Thermal Spray Conference, 1993, pp. 457–462.
11. *Idem., Atomization and Sprays* **4** (1994) 369–384.
12. PASANDIDEH-FARD and J. MOSTAGHIMI, "Droplet Impact and Solidification in a Thermal Spray Process: Droplet-Substrate Interactions," Proceedings of the 9th National Thermal Spray Conference, 1996, pp. 637–646.
13. S. INADA, *Journal of Chemical Engineering of Japan* **21** (1998) 582–588.
14. T. WATANABE, I. KURIBAYASHI, T. HONDA and A. KANZAWA, *Chemical Engineering Science* **47** (1992) 3059–3065.
15. S. INADA and W.-J. YANG, *Experimental Heat Transfer* **7** (1994) 93–100.
16. H. FUKANUMA and A. OHMORI, "Behavior of Molten Droplets Impinging on Flat Surfaces," Proceedings of the 7th National Thermal Spray Conference, 1994, 563–568.
17. B. KANG, Z. ZHAO and D. POULIKAKOS, *ASME Journal of Heat Transfer* **116** (1994) 436–445.
18. T. BENNETT and D. POULIKAKOS, *J. Mater. Sci.* **29** (1994) 2025–2039.
19. S. CHANDRA and C. T. AVEDISIAN, *Proceedings of the Royal Society A* **432** (1991) 13–41.
20. M. PASANDIDEH-FARD, Y. M. QIAO, S. CHANDRA and J. MOSTAGHIMI, *Physics of Fluids* **8** (1996) 650–659.
21. A. F. MILLS "Heat Transfer" (Irwin, Boston MA, 1992) pp. 183–186.
22. H. S. CARSLAW and J. C. JAEGER, "Conduction of Heat in Solids" (Oxford University Press, London, 1959) pp. 87–89.
23. N. B. VARGAFTIK, "Handbook of Physical Properties of Liquids and Gases" (Hemisphere Publishing Co., Washington, 1975).
24. C. MUNDO, M. SOMMERFIELD and C. TROPEA, *International Journal of Multiphase Flow* **21** (1995) 151–173.
25. C. D. STOW and M. G. HADFIELD, *Proceedings of the Royal Society A* **373** (1981) 419–441.
26. P. SAVIC and G. T. BOULT, The fluid flow associated with the impact of liquid drops with solid surfaces, *National Research Council of Canada*, Report No. MT-26, (1955).
27. R. F. ALLEN *Journal of Colloid and Interface Science* **51** (1975) 350–351.
28. E. GUTIERREZ-MIRAVETE, E. J. LAVERNIA, G. M. TRAPAGA, J. SZEKELY and N. J. GRANT, *Met. Trans. A* **20A** (1989) 71–85.
29. *Idem., ibid.* **26** (1983) 1095–1098.

Received 5 January 1997
and accepted 24 February 1999